Int. J. Electrochem. Sci., 17 **(2022)** Article Number: 220539, doi: 10.20964/2022.05.41

International Journal of
ELECTROCHEMICAL
SCIENCE
www.electrochemsci.org

Short Communication

Effect of Annealing Temperature on Microstructure and Corrosion Behavior of CoCrNi Medium-entropy Alloy in 3.5 wt.% NaCl Solution

Feng He[1], *Zhongping Le*[1,*], *Min Zhu*[1,*], *Li Liu*[2], *Xiang Zhang*[3], *Guotu Zhu*[4]

[1] School of Mechanical Engineering & Automation, Zhejiang Sci-Tech University, Hangzhou 310018, PR China
[2] Interplex Electronic (HZ) Co., Ltd., Hangzhou 310018, China
[3] Zhejiang Zheneng Natural Gas Operation Co., Ltd., Hangzhou 310052, China
[4] Changshan Chengxin bearing Co., Ltd., Changshan 324000, China
[*]E-mail: zmii666@126.com, lelezp@126.com

Received: 8 February 2022 / *Accepted:* 4 March 2022 / *Published:* 5 April 2022

This work investigates the effect of annealing temperature on corrosion performance of CoCrNi medium-entropy alloy (MEA) in 3.5 wt.% NaCl solution. The corrosion property of CoCrNi MEA improves with the increase of annealing temperature. The corrosion behavior of the annealed MEA is associated with grain size and passive film. The difference in electrochemical activity between substrate and oxide inclusion is the main cause of micro-galvanic corrosion, which facilitates the dissolution of matrix and induces the formation of pits. The matrix (anode) and oxide inclusion (cathode) both experience the selective dissolution of Co, except that oxide also undergoes the marked dissolution of Ni.

Keyword: Medium-entropy alloy, Corrosion, Microstructure, Annealing treatment

1. INTRODUCTION

Medium-entropy alloys (MEAs) as a novel concept in alloy design, it is different from traditional alloys with one or two main elements, MEAs have multi-elements as their main constituents [1], which enables them to possess excellent performances[2]. The mechanical properties of CoCrNi MEA have attracted many attentions. Moravcik et al. [3] found that the CoCrNi MEA produced by powder metallurgy showed superior mechanical properties compared with high-strength steel and other HEAs, such as FeMnCoCrNi, CoCrFeNi, $Fe_{40}Mn_{27}Ni_{26}Co_5Cr_2$, $Fe_{40.4}Ni_{11.3}Mn_{34.8}Al_{7.5}Cr_6C_1$, etc. Lu et al. [4] studied the low-cycle fatigue behavior of the CoCrNi MEA and CoCrFeMnNi HEA at room

temperature, which showed that the former had higher strength, lower inelastic strain and longer life. Wu et al. [5] showed that the CoCrNi MEA had outstanding mechanical properties compared with typical CoCrFeMnNi HEA and most multi-phase alloys at low temperature and room temperature. Laplanche et al. [6] revealed that nano-twins appeared in CoCrNi, which provided high and stable work hardening, with the result that MEA had better mechanical properties than CrMnFeCoNi HEA. As mentioned above, the CoCrNi MEA shows superior mechanical properties. Hence, it may have a wide application prospect.

At present, few literatures on the corrosion behavior of CoCrNi are mainly concentrated on acidic and alkaline environments. Wang [7] found that CoCrNi exhibited superior corrosion resistance in H_2SO_4 than 304 stainless steel. Conversely, the MEA experienced more severe corrosion in NaOH solution. Zhang et al. [8] investigated the corrosion of a selective laser-melted (SLM) CoCrNi MEA with its casting alloy, and found that surface defects were the critical factors determining the corrosion performance. However, the study on the influence of microstructure on corrosion behavior of MEA in a simulated marine environment has not been reported. Therefore, the microstructure of MEA is adjusted by annealing treatment to study the influence of microstructure on its corrosion behavior.

2. EXPERIMENTAL

2.1. Material and solution

The CrCoNi MEA ingot was fabricated by high-purity elements (Co, Cr, and Ni) in an induction suspension furnace at 1700℃ under an argon atmosphere, then cooled for 30 minutes. The above process was repeated four times to guarantee homogenous distribution of elements within the ingot. Subsequently, the as–cast MEA was machined into a dimension of 10 mm × 10mm × 3mm. The annealing treatment procedure was as follows: the MEA sample was heated in a muffle furnace at various temperatures of 750℃, 850℃, and 950℃ for 1.5 h under an air atmosphere, respectively, followed by water quenched. Different annealed specimens were sealed with epoxy resin, and left a surface of 1 cm^2 for testing. These specimens were ground gradually using water sandpaper from 400 to 2000 grit, then cleaned with anhydrous alcohol and deionized water, and dried in the cool air.

In this work, 3.5% NaCl solution was chosen as a corrosion medium. Various annealed MEA specimens were etched by the reagent solution of 2 g $FeCl_3$ + 5 mL HCl + 1 mL HNO_3 + 10 mL H_2O. The microstructure detail of different specimens was analyzed via scanning electron microscope (SEM, FEI-quanta250), and energy dispersive spectrometer (EDS).

2.2 Electrochemical tests

The electrochemical test was conducted on the CHI660 electrochemical workstation with the conventional three-electrode system. The MEA specimen was acted as the working electrode, with the saturated calomel electrode (SCE) as the reference electrode and platinum plate as the counter electrode. Prior to testing, different HEA samples were soaked in the solution for 1.5h to achieve the

pre-passivation state. Subsequently, the open-circuit potential (OCP) was tested for 30 min, then the electrochemical impedance spectroscopy (EIS) was measured. The EIS curve was measured in the frequency range of 100kHz-10mHz with10mV interference signal. The potentiodynamic polarization curve was performed with a sweep rate of 1 mV/s, ranging from -1 V to 0.8 V.

For the Mott-Schottky curve, firstly, passive films were grown on various annealed specimens by potentiostat polarization at a potential of 0.2V for 2h.Then the Mott-Schottky curve was measured at a fixed frequency of 1 kHz in the range of -1 V ~ 0.8 V with a step length of 50 mV. Through this, the difference in the anti-corrosion resistance of MEA specimens annealed for various temperatures can be clarified from the protective performance of passive films.

2.3 Immersion test

Various annealed MEA specimens were thoroughly rinsed and dried, weighed, then immersed in the solution for 7 days. At the end of the test, the average corrosion rates of different annealed specimens were obtained by the weight loss data. The corrosion morphologies were analyzed by SEM and EDS. All tests were conducted at 30°C.

3. RESULTS

3.1 Microstructure analysis

Fig. 1 exhibits the microstructure and EDS results of CoCrNi MEA annealed at different temperatures. In Fig. 1(e), the distribution of component elements in the grain boundary (GB) and grain interior is homogenous, without segregation. The average grain sizes of the MEA annealed at different temperatures are 75 μm, 116 μm and 135 μm (Fig. 1(d)). It is well known that due to the preferential distribution of defects and impurities in the GB region, the grain boundary shows the relatively terrible passivation property. Therefore, the decreased grain size causes an increasing volume fraction of GB, which implies that the electrochemical reaction in the GB region is more intense [9]. Hence, the MEA with larger grain size has more excellent anti-corrosion property. Fig.1(a-c) show that the MEA mainly consists of a typical single-phase FCC structure. Moreover, according to EDS results (Fig.2(a-e)) of black particles in the red circle marked in Fig. 1(a-c) (point 2 in Fig. 2(a)), the particle is named oxide inclusion, which is constituted of O, Al, Ti, Cr, Co, Ni, and C elements. The existence of Al, Ti, O, and C elements may be caused by metallurgical contamination [10].

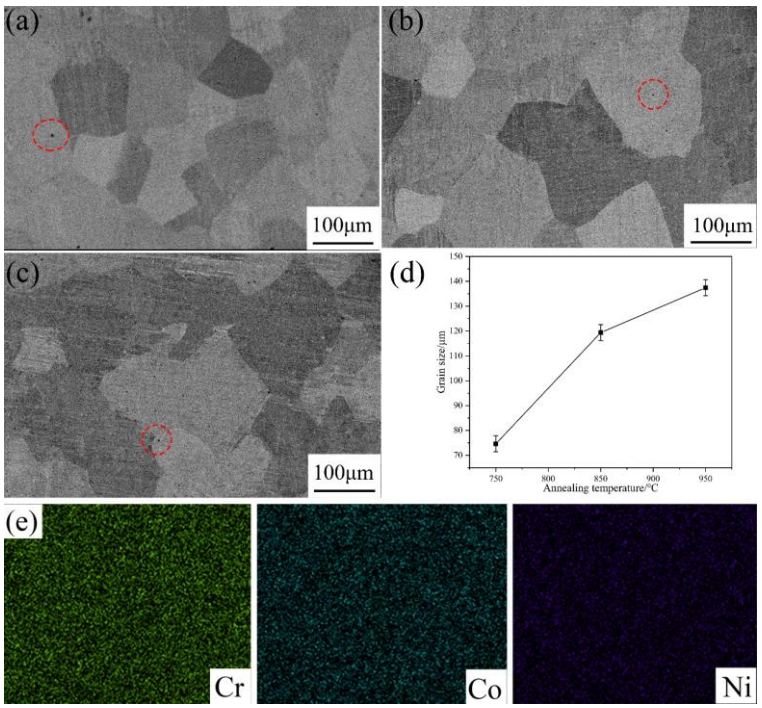

Figure 1. Microstructures (a-750℃, b-850℃, c-950℃), grain size (d) of CoCrNi MEA annealed at different temperatures and the EDS mapping (e).

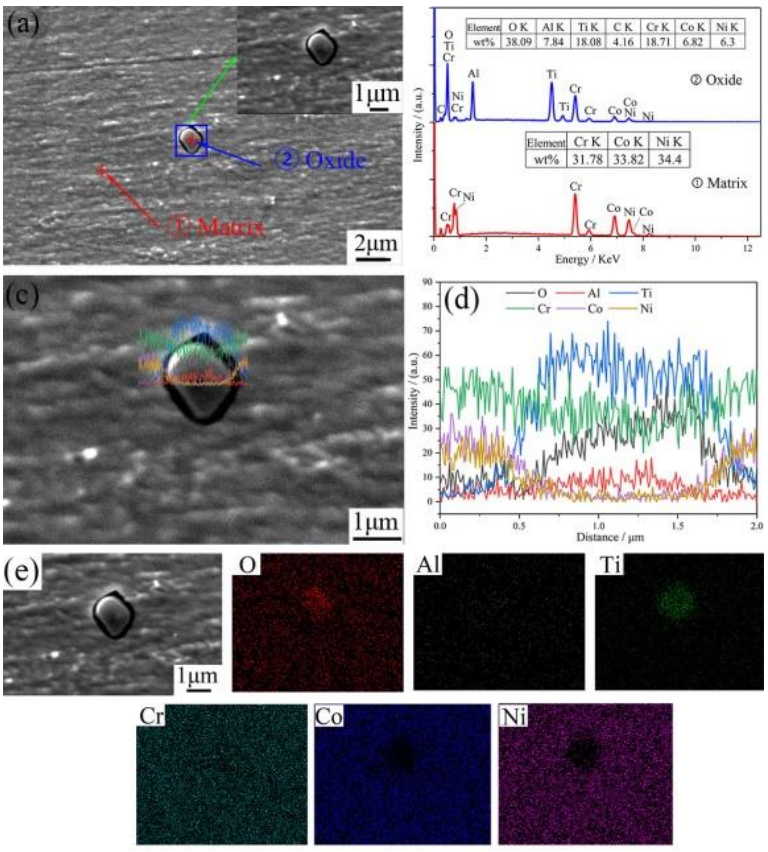

Figure 2. SEM morphologies and EDS analysis results of oxide inclusions within the microstructure of the MEA

3.2 Electrochemical measurements

In Fig. 3(a), a negative shift in open-circuit potential means that the corrosion tendency of the MEA increases with decreasing annealing temperature. Fig. 3(b-c) exhibits the EIS curves of different annealed samples. The classical capacitive loop characteristics suggest that the corrosion behavior is kinetically controlled by charge transfer process [7]. Additionally, the diameter of capacitive loop reveals the corrosion resistance of various MEA samples. The larger arc diameter means superior anti-corrosion property. Thus, the Nyquist curves demonstrate that the anti-corrosion resistance of the CoCrNi increases as annealing temperature rises.

In Fig. 4, the equivalent electric circuit was used to fit the EIS data. Among them, R_s is the electrolyte resistance, Q_f symbolizes the passive film capacitance, R_f denotes the passive film resistance, Q_{dl} represents the nonideal double-layer capacitance and R_{ct} is the charge transfer resistance at the solution/electrode interface. According to the EIS fitting result (Fig. 3(d)), the lower R_f and R_{ct} values suggest that the passive film formed on the MEA annealed at 750℃ has more activated sites, with poor uniformity and compactness. Thus, the 750℃-annealed MEA exhibits the worst corrosion resistance.

Fig. 3(e) displays the potentiodynamic polarization curves of different annealed CoCrNi samples. The curves gradually shift to the right with an increased annealing temperature. In Fig. 3(f), the fitted passive current densities (i_p) of CoCrNi annealed at 750℃, 850℃, 950℃ are 26.8×10^{-5}A·cm^{-2}, 9.644×10^{-5}A·cm^{-2}, and 4.658×10^{-5}A·cm^{-2}. The smaller the i_p is, the slower the dissolution rate of passive film, indicating that the passive film of CoCrNi MEA annealed at 950℃ can effectively protect the metal matrix from the penetration of corrosive ions. Moreover, the critical pitting potential (E_p) increases as annealing temperature rises, which reflects that the pitting sensitivity of CoCrNi annealed at 750℃ is largest.

The semiconductor property of passive films on various annealed specimens was measured by Mott-Schottky curve. The correlation between space charge capacitance (C) and applied electrode potential (E) was exhibited as follows [11,12]:

$$\frac{1}{C^2} = \pm\frac{2}{eN\varepsilon\varepsilon_0}\left(E - E_{FB} - \frac{kT}{e}\right) \quad (1)$$

where the positive sign (+) and negative sign (-) denote the n/p type semiconductors. ε is the dielectric constant, in this paper, ε = 12 [13,14]. ε_0 is the vacuum dielectric constant (8.854×10^{-14} F·cm^{-1}), E is the applied electrode potential, k represents the Boltzmann constant (1.38×10^{-23} J·K^{-1}), E is the electron charge (1.602×10^{-19} C), E_{FB} is the flat band potential, and T is the Kelvin temperature (K). N is the carrier concentration (N_D is the donor density, and N_A is the acceptor density), and its value was calculated according to the following formula:

$$N = \frac{2}{em\varepsilon\varepsilon_0} \quad (2)$$

Donor (N_D) and acceptor densities (N_A) were calculated by the positive and negative slopes (m) of linear segments in Fig. 3(g). The result is displayed in Fig. 3(h), the N_A and N_D values of the MEA annealed at 750℃ are the largest, whereas the 950℃-annealed sample has the lowest values. According to the point defect model, the negative and positive slope regions mean that the film shows the p and n-type semiconductor characteristics, including the main defects of cation and oxygen

vacancies [15]. Thus, the larger the values of N_A and N_D, the faster the charge transfer that occurs in the passive film, that is, the more intense the electrochemical reaction, which indicates that the passive film of the MEA annealed at 750℃ has inferior corrosion resistance.

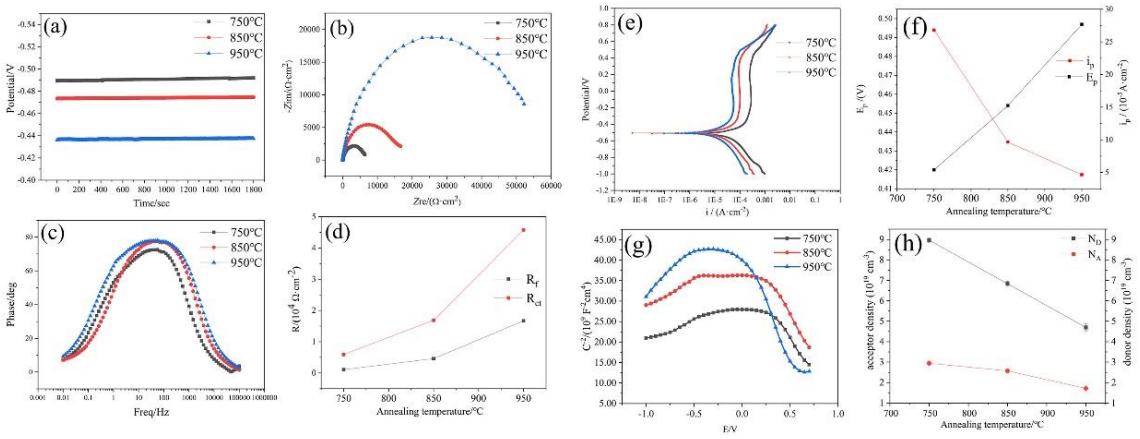

Figure 3. Electrochemical results of CoCrNi MEA annealed at different temperatures: open-circuit potential (a), EIS curve (b-c) and R_f, R_{ct} (d), polarization curve (e) and E_p, i_p (f), Mott-Schottky curve (g) and N_A, N_D (h).

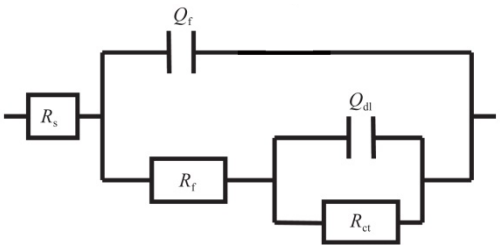

Figure 4. Equivalent electric circuit for fitting EIS data.

3.3 Immersion test

Fig. 5(a-c) exhibits the surface corrosion morphologies of CoCrNi MEA annealed at different temperatures after soaking in 3.5% NaCl solution for 7 days. 750℃-annealed specimen was seriously corroded, with the relatively dense pits. And the corrosion degree of the specimen annealed at 950°C is the slightest. As seen in Fig. 5(d), 950°C-annealed sample has the lowest corrosion rate, followed by 850°C and 750°C. Therefore, the corrosion resistance of CoCrNi MEA is enhanced as annealing temperature increases.

The EDS results of Fig. 5(e-f) demonstrate Co content in the pitting region (point 2) is lower than that in matrix (point 1). This indicates that the pits distributed on MEA surface are caused by selective dissolution of Co element. Furthermore, as shown in Fig. 5(g-h), pitting corrosion (point 2) occurs around the oxide inclusion (point 3). The reason for this phenomenon is probably due to the potential difference between the matrix and inclusion, resulting in micro-galvanic corrosion. After the formation of micro-galvanic cells with inclusions and matrix as cathode and anode respectively, not

only the matrix undergoes electrochemical dissolution, but also the inclusions react with the solution, resulting in a relatively remarkable reduction of the elements, which may be the cause for the hole within the oxide inclusion region (point 3). In addition, the variation in the element contents within oxide inclusion reflects that the selective dissolution of Co and Ni elements results in the dissolution of inclusion.

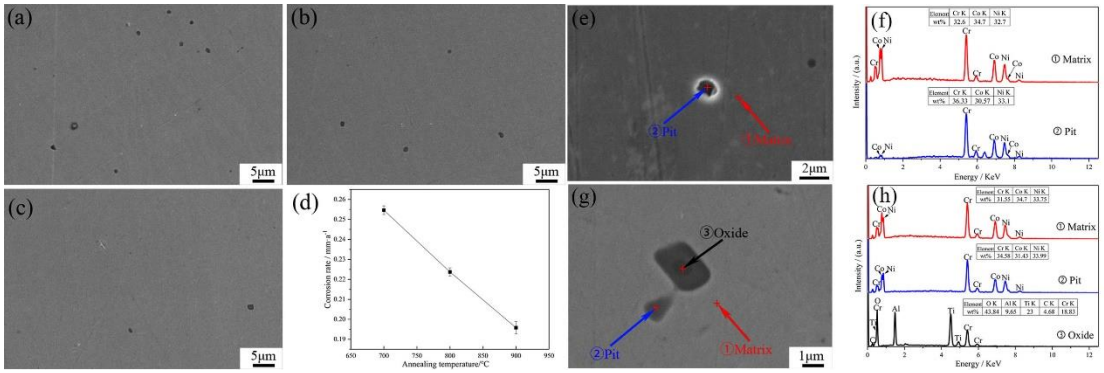

Figure 5. Corrosion morphologies (a-750℃, b-850℃, c-950℃), corrosion rates (d) of CoCrNi MEA annealed at different temperatures, and the related EDS results (e-h)

Based on the variation of element content, the possible electrochemical reactions [16,17] are listed below:

Cathodic reaction on oxide inclusion (Eq.1):

$$O_2 + 2H_2O + 4e^- \rightarrow 4OH^- \quad (1)$$

Anodic reaction on the matrix (Eq.2):

$$Co \rightarrow Co^{2+} + 2e^- \quad (2)$$

Dissolution of oxide inclusion (Eqs.2, 3):

$$Ni \rightarrow Ni^{2+} + 2e^- \quad (3)$$

4. CONCLUSIONS

The influence of annealing temperature on the corrosion behavior of CoCrNi MEA in 3.5 wt.% NaCl solution was explored, and the main conclusions are as follows:

As annealing temperature increases, the anti-corrosion resistance of MEA improves. The grain size and surface passive film of CoCrNi MEA annealed at various temperatures determine the difference of anti-corrosion property. The difference in electrochemical activity between substrate and oxide inclusion is the main cause of micro-galvanic corrosion, which facilitates the dissolution of matrix and induces the formation of pits. And matrix (anode) and oxide inclusion (cathode) both experience the selective dissolution of Co, except that oxide also undergoes the marked dissolution of Ni.

ACKNOWLEDGEMENTS
This work was supported by the National Natural Science Foundation of China (No. 51871026) and National Material Environmental Corrosion Infrastructure.

References

1. B. Gludovatz, A. Hohenwarter, K.V. Thurston, H. Bei, Z. Wu, E.P. George and R.O. Ritchie, *Nat. Commun.*,7(2016)No.10602.
2. S. Praveen, W.B. Jae, P.Asghari-Rad, J.M. Park and H.S. Kim, *Mat. Sci. Eng. R.,* 734(2018)338.
3. I. Moravcik, J. Cizek, Z. Kovacova, J. Nejezchlebova, M. Kitzmantel, E. Neubauer, I. Kubena, V. Hornik and I.Dlouhy, *Mater. Sci. Eng. A,* 701(2017)370.
4. K. Lu, A. Chauhan, M. Walter, A.S. Tirunilai, M. Schneider, G. Laplanche, J. Freudenberger, A. Kauffmann, M. Heilmaier and J. Aktaa, *Scr. Mater.,* 194(2021)No. 113667.
5. Z. Wu, H. Bei, F. Otto, G.M. Pharr and E.P. George, *Intermetallics,* 46(2014)131.
6. G. Laplanche, A. Kostka, C. Reinhart, J. Hunfeld, G. Eggeler and E.P. George, *Acta Mater.,* 128(2017)292.
7. J.Y. Wang, W.H. Li, H.L. Yang, H. Huang, S.X. J, J.M. Ruan and Z.L. Liu, *Corros. Sci.,* 177 (2020) No. 108973.
8. Z. Zhang, T. Yuan and R. Li, *J. Alloy. Compd.,* 864(2021)No. 158105.
9. B. Heine and R. Kirchheim, *Corros. Sci.,* 31(1990)533.
10. I. Moravcik, S.N. Peighambardoust, A. Motallebzadeh, L.G. Moravcikova Gouvea, C. Liu, M.J. Prabhakar, I. Dlouhy and Z.M. Li, *Mater. Charact.,* 172 (2020) No.110869.
11. H.X. Guo, B.T. Lu and J.L. Luo, *Electrochim. Acta,* 52(2006)1108.
12. Q. Liu, X.R. Zhang, W.H. Zhou, R.N. Ma, A. Du, Y.Z. Fan, X. Zhao and X.M. Cao, *Corros. Sci.,* 174(2020)No. 108846.
13. H. Luo, S.W. Zou, Y.H. Chen, Z.M. Li, C.W. Du and X.G. Li, *Corros. Sci.,* 163(2020)No.108287.
14. M. Zhu, B.Z. Zhao, Y.F. Yuan, S.Y. Guo and G.Y. Wei, *J. Electroanal. Chem.,* 882(2021) No.115026.
15. H. Luo, Z.M. Li, A.M. Mingers and D. Raabe, *Corros. Sci.,* 134(2018)131.
16. H. Feng, H.B. Li, X.L. Wu, Z.H. Jiang, S. Zhao, T. Zhang, D.K. Xu, S.C. Zhang, H.C Zhu, B.B. Zhang and M.X. Yang, *Mater. Sci. Technol.,* 34(2018)1781.
17. Q. Li, X.J. Xia, Z.B. Pei, X.Q. Cheng, D.W. Zhang, K. Xiao, J. Wu and X.G. Li, *npj Mater. Degrad.,* 6**(**2022)1.